Cell stress response impairs de novo NAD+ biosynthesis in the kidney

Yohan Bignon, Anna Rinaldi, Zahia Nadour, Virginie Poindessous, Ivan Nemazanyy, Olivia Lenoir, Baptiste Fohlen, Pierre Weill-Raynal, Alexandre Hertig, Alexandre Karras, et al.

JCI insight

Cell stress response impairs de novo NAD$^+$ biosynthesis in the kidney

Yohan Bignon, … , Pietro E. Cippà, Nicolas Pallet

JCI Insight. 2021. https://doi.org/10.1172/jci.insight.153019.

Research In-Press Preview **Metabolism** **Nephrology**

The biosynthetic routes leading to de novo Nicotinamine Adenine Dinucleotide (NAD+) production are involved in acute kidney injury (AKI) with a critical role for Quinolinate Phosphoribosyl Transferase (QPRT), a bottleneck enzyme of de novo NAD$^+$ biosynthesis. However, the molecular mechanisms determining reduced QPRT in AKI, and the role of impaired NAD$^+$ biosynthesis in the progression to chronic kidney disease (CKD) are unknown. We demonstrate that a high urinary quinolinate to tryptophan ratio, an indirect indicator of impaired QPRT activity and reduced de novo NAD$^+$ biosynthesis in the kidney, is a clinically applicable early marker of AKI after cardiopulmonary bypass, and is predictive of progression to chronic kidney disease (CKD) in kidney transplant recipients. We also provide evidence that the Endoplasmic Reticulum (ER) stress response impairs de novo NAD$^+$ biosynthesis by repressing QPRT transcription. In conclusion, NAD$^+$ biosynthesis impairment is an early event in AKI embedded with the ER stress response, and persistent reduction of QPRT expression is associated with AKI to CKD progression. This defines non-invasive metabolic biomarkers of kidney injury with prognostic and therapeutic implications.

Cell stress response impairs de novo NAD^+ biosynthesis in the kidney

Yohan Bignon[1,*], Anna Rinaldi[2,*], Zahia Nadour[1,3,*], Virginie Poindessous[1], Ivan Nemazanyy[4], Olivia Lenoir[5], Baptiste Fohlen[6], Pierre Weill-Raynal[6], Alexandre Hertig[7], Alexandre Karras[1,8], Pierre Galichon[9], Maarten Naesens[10], Dany Anglicheau[11], Pietro E Cippà[2,**], Nicolas Pallet[1,3,7,**]

1. Université de Paris, INSERM UMRS1138, Centre de Recherche des Cordeliers, F-75006 Paris, France
2. Department of Medicine, Division of Nephrology, Ente Ospedaliero Cantonale, Lugano, Switzerland
3. Service de Biochimie, Assistance Publique Hôpitaux de Paris, Hôpital Européen Georges Pompidou, F-75015, Paris, France
4. Plateforme d'analyses du métabolisme, Structure Fédérative de Recherche Necker, INSERM US24/CNRS UMS3633, F-75015, Paris, France
5. Université de Paris, Inserm UMRS970, Paris centre de recherche cardiovasculaire (PARCC), F-75015, Paris, France.
6. Service d'Anesthésie Réanimation Chrirugicale, Assistance Publique Hôpitaux de Paris, Hôpital Européen Georges Pompidou, F-75015, Paris, France
7. Service de Néphrologie, Hôpital Foch, Suresnes, France
8. Service de Néphrologie, Assistance Publique Hôpitaux de Paris, Hôpital Européen Georges Pompidou, F-75015, Paris, France
9. INSERM UMRS1155, Maladies Rénales Fréquentes et Rares: des Mécanismes Moléculaires à la Médecine Personnalisée, Sorbonne Université, Paris, France
10. Department of Microbiology, Immunology and Transplantation, KU Leuven, Leuven, Belgium
11. Service de Néphrologie et Transplantation, Assistance Publique Hôpitaux de Paris, Hôpital Necker, F-75015, Paris, France

*: co first authors
**: co senior authors

Conflict of interest statement: the authors have declared that no conflict of interest exists.

Running title: Quinolinate phosphoribosyl transferase expression upon kidney injury

Correspondence
Pr. Nicolas Pallet
INSERM UMRS1138, Centre de Recherche des Cordeliers
15 rue de l'Ecole de Médecine
75006 Paris, France
Phone: +33156092435; Fax: +33156093393
E-mail: Nicolas.pallet@aphp.fr

Abstract

The biosynthetic routes leading to de novo Nicotinamine Adenine Dinucleotide (NAD^+) production are involved in acute kidney injury (AKI) with a critical role for Quinolinate Phosphoribosyl Transferase (QPRT), a bottleneck enzyme of de novo NAD^+ biosynthesis. The molecular mechanisms determining reduced QPRT in AKI, and the role of impaired NAD^+ biosynthesis in the progression to chronic kidney disease (CKD) are unknown.

We demonstrate that a high urinary quinolinate to tryptophan ratio, an indirect indicator of impaired QPRT activity and reduced de novo NAD^+ biosynthesis in the kidney, is a clinically applicable early marker of AKI after cardiac surgery and is predictive of progression to chronic kidney disease (CKD) in kidney transplant recipients. We also provide evidence that the Endoplasmic Reticulum (ER) stress response may impair de novo NAD^+ biosynthesis by repressing QPRT transcription.

In conclusion, NAD^+ biosynthesis impairment is an early event in AKI embedded with the ER stress response, and persistent reduction of QPRT expression is associated with AKI to CKD progression. This defines non-invasive metabolic biomarkers of kidney injury with prognostic and therapeutic implications.

Introduction

Nicotinamide adenine dinucleotide (NAD^+) is a cofactor involved in oxido-reduction reactions and serves as an energy transfer intermediate in multiple metabolic pathways (1). NAD^+ is an important cosubstrate for histones deacetylases (sirtuins) and poly(ADP-ribose) polymerases (PARPs), which regulate several aspects of cellular homeostasis (1). Cellular NAD^+ reduction in aging and in association with several diseases contributes to overall fitness decline and to a lower resistance to cell stress. Conversely, increasing NAD^+ content can prolong health and life span in experimental organisms (2),(3). Recent experimental and clinical data demonstrated a critical role for NAD^+ homeostasis in acute kidney injury (AKI) (4),(5),(6),(7). Proximal tubular cells (PTCs) are highly metabolically active and their survival and function depend on the possibility to couple their energetic needs to the regulation of energy generation, antioxidant responses, and mitochondrial biogenesis and quality control, all of which rely on cytosolic and mitochondrial NAD^+ (5),(8). NAD^+ is continuously degraded, and stable NAD^+ cellular concentrations are maintained by constant new supply through the nicotinamide salvage pathway (nicotinamide is generated as a by-product of enzymatic activities) and biosynthetic pathways (**Suppl. Figure 1**). NAD^+ biosynthesis involves diverse dietary sources, including nicotinic acid, nicotinamide, nicotinamide riboside, and tryptophan. The de novo pathway converts dietary tryptophan to NAD^+ in eight steps with the last catalyzed by quinolinate phosphoribosyltransferase (QPRT). Reduction in QPRT activity during AKI is considered critical in NAD^+ biosynthetic impairment (6), but the molecular mechanisms determining reduced QPRT upon kidney injury and its role in long-term outcomes after AKI remain unclear. The clinical relevance a non-invasive monitoring of QPRT activity in patients with a kidney disease is not established.

Results

Impaired NAD^+ biosynthesis is a very early event in AKI

A previous study showed that quinolinate accumulates as a consequence of reduced QPRT activity and that urinary quinolate/tryptophan ratio (uQ/T) is elevated in AKI (6). Metabolic profiling of urine samples collected at baseline and the day after cardio pulmonary bypass (CPB) in 41 cardiac surgery patients (**Supp. Figure 3** for metabolomic data and **Suppl. Table 2** for clinical data), including 11 patients (26%) developing AKI in the 7 days following CPB according to KDIGO criteria, confirmed that uQ/T was higher at day 1 after surgery in patients developing AKI, whereas at baseline, the levels were the same (**Figure 1A**), and severity of AKI correlated with uQ/T levels at day 1 (**Figure 1B**). uQ/T was one of few urinary metabolic parameters significantly discriminating AKI at day 1 after surgery (but not at baseline) in this cohort (**Figure 1C**). uQ/T on day 1 after cardiac surgery predicted AKI with a higher accuracy than other AKI biomarkers, including kidney injury molecule 1 (KIM-1) or neutrophil gelatinase associated lipocalin (NGAL) (**Figure 1D**). In a multivariate analysis, uQ/T measured the day after CPB was an independent predictor of the occurrence of AKI (**Suppl. Table 3** and **4** for uni and multivariate analyses). Urinary QPRT transcripts (urinary gene expression patterns reflect the dynamics of biopsy genes signatures (9),(10),(11)) were negatively correlated with uQ/T levels, in line with the fact that elevated uQ/T is an indirect marker of reduced QPRT activity (**Figure 1E**). QPRT mRNA levels were significantly reduced in the first -after ischemia-reperfusion injury (IRI) in protocol biopsies obtained in 42 kidney transplant recipients (KTR) before and after reperfusion (12) (**Figure 1F**). QPRT transcripts levels were highly anticorrelated with HAVCR1 (the gene encoding KIM-1) transcripts (**Figure 1G**), suggesting that patients with more severe AKI in the post transplantation biopsy had more pronounced QPRT reduction after reperfusion. Finally, in a mouse model of bilateral IRI (13), Qprt achieved the lowest level within 24 h after IRI (**Figure 1H**). Thus, reduced QPRT transcription and activity is an early event associated with AKI. Indirectly determined by uQ/T in a clinical context, this is the first metabolic change predictive of AKI detectable by urinary metabolic profiling.

QPRT reduction is associated with progression to chronic kidney disease

To investigate the long-term impact of the early reduction of de novo NAD^+ biosynthesis associated with IRI, we performed a targeted urinary metabolic profiling in 237 KTR 10 days after transplantation (**Suppl. Table 5** for clinical data). Hierarchical clustering according to metabolic profiling identified 3 clusters (**Figure 2A**). Donor related parameters, such as age, history of hypertension, renal function, or death from stroke (ie. Extended Criteria Donor kidneys), were balanced among the clusters (**Suppl. Figure 4A** and **B**), but cluster 2 was enriched with patients who undergone more severe ischemic injury, as indicated by longer cold ischemia time, higher serum creatinine the day of urine sampling, and higher frequency of delayed graft function episodes (need for at least on dialysis session during the 7 days after transplantation) and a higher number of dialysis sessions (**Figure 2B** to **D** and **Suppl. Figure 4C**). Among the urinary metabolites that best characterized cluster 2, quinolinate and uQ/T had the largest and significant size effect (**Figure 2E** and **Suppl. Table 6** for the list of metabolites). Critically, multivariate models integrating all variables associated with graft outcomes showed that high uQ/T 10 days after transplantation was an independent predictor of allograft function 3 and 12 months after transplantation (**Tables 1 and 2**).

To investigate the role of QPRT along the transition from AKI to CKD, we took advantage of the previously reported cohort of 42 KTR followed by bulk RNAseq in protocol biopsies obtained 3 and 12 months after transplantation (12). A computational model to characterize the transcriptional transition from AKI to CKD has been developed, based on the principle that the progression to fibrosis is a transitional process from acute injury to fibrosis (12) (see **Methods**). According to this computational model, QPRT was progressively reduced along the transition to CKD (**Figure 2F**), a finding confirmed by immunohistochemistry in kidney biopsies obtained from patients with CKD (**Figure 2G**), by the correlation between renal function and QPRT transcripts levels in urinary cell pellets in a cohort of 55 CKD patients (**Figure 2H** and **Suppl. Table 7** for clinical data), and by a lower expression of QPRT transcripts in tubular

human diabetic tissues (14) (**Figure 2I**). Thus, persistent QPRT reduction and impaired de novo NAD^+ biosynthesis after AKI is a feature of the transition to chronic renal damage.

ER stress reduces de novo NAD^+ biosynthesis in the kidney

We next investigated the potential mechanisms determining the reduction of NAD^+ biosynthetic activity upon AKI. Among the several factors involved in the early transcriptional response to AKI, we focused on the endoplasmic reticulum (ER) stress response, which is known to be activated in the early kidney injury response in mouse (15),(16) and human (17). We modeled the interaction between ER stress and NAD^+ biosynthesis in PTCs by performing *in vitro* studies in the Human Kidney 2 (HK2) cell line, a proximal tubule-derived cell line expressing QPRT (**Suppl. Figure 5**). In line with this, analysis of mouse single nucleus RNA sequencing datasets indicated that Qprt is almost exclusively expressed in PTCs (**Figure 3A)**, which is in line with transcriptomic and proteomic data in micro dissected tubules in rats (18),(19) (**Suppl. Figure 6A** and **B**), and supported by an immunohistochemistry study on normal human kidney (**Figure 3B**).

In an unbiased approach, we induced ER stress with tunicamycin (Tun), an inhibitor of GlcNAc phosphotransferase that promotes ER stress and activates the Unfolded Protein response (UPR) (**Suppl. Figure 7**), and we performed metabolomic analysis in the cell lysate. ER stress profoundly reshaped the intracellular metabolic profile of HK2 cells (**Figure 3C**). Among the metabolites strongly enriched in response to ER stress we found asparagine (ER stress induces asparagine synthase (20),(21)), and quinolinate (**Figure 3D** and **Suppl. Table 8A** for the list of metabolites). Similar results were obtained after ER stress induction with Brefeldin A (BFA) (**Suppl. Figure 7**), a lactone that inhibits protein transport from the ER to the Golgi complex (**Suppl. Figure 8** and **Suppl. Table 8B** for the list of metabolites). ER stress induced by Tun or BFA reduced NAD^+ intracellular contents (**Figure 3E)**. This process was inhibited by TES1025 (**Figure 3F**), an inhibitor of the α-amino-β-carboxymuconate-ε-semialdehyde decarboxylase (ACMSD), indicating ER stress represses de novo NAD^+ synthesis since ACMSD decreases the proportion of substrates able to undergo spontaneous cyclization into

quinolinic acid (**Suppl. Figure 1**). Importantly, the decrease in NAD^+ intracellular content was unlikely a consequence of accelerated consumption of NAD^+ by PARPs, because ER stress was associated with PARP cleavage and a defective PARylation activity (**Figure 3G to I**). Note that Etoposide, used as a positive control to promote apoptosis, does not induces ER stress and does not affect QPRT expression (**Figure 3G and H**). We observed a slight increase in expression of the transcripts of the ectonuclease CD38 upon ER stress in HK2 (**Figure 3J**). CD38, an ecto-enzyme capable of reducing extracellular NAD^+ precursors availability (22), could theoretically participate to the decrease in NAD^+ contents observed in ER stressed cells, albeit the culture medium used (Dulbecco's Modified Eagle Medium) contain high and likely saturating concentrations of nicotinamide (4 mg/L). These results suggest that ER stress may be involved in NAD^+ biosynthetic impairment, and that quinolinate accumulation is consistent with a reduction in the de novo biosynthetic pathway activity.

QPRT expression is repressed in response to kidney injuries associated with ER stress

A diminished expression of Qprt was found in several models of kidney injuries associated with ER stress (using DNA Damage Inducible Transcript 3 (DDIT3), also known as C/EBP homologous protein (CHOP)), as a surrogate marker (23), for instance injection of Tun; a transgenic mouse model expressing mutant uromodulin (UmodC147W/+) that accumulates in the ER lumen; and streptozotocin-induced diabetic nephropathy (**Figure 4A** to **C**). In addition, in the first hours after IRI in mice, single nucleus RNA sequencing indicated that PTCs displayed a fundamental change of their transcriptional profile with the expression of established injury markers (e.g. Havcr1), and the parallel loss of classical differentiation markers (eg. Lrp2, encoding megalin), leading to the characterization of novel PTCs clusters (called PT1 to 3), which were referred to as “injured proximal tubule” (**Figure 4D** and **E**) and **Suppl. Figure 6C to E)** (8). PTCs in the early damaged state displayed low levels of Qprt (**Figure 4F**) associated with high levels of the ER stress marker Ddit3 (**Figure 4G)**, indicating that the ER stress response is engaged in PTCs following IRI, and that in this condition, Qprt expression is repressed.

ER stress induced by Tun, BFA, thapsigargin (Tg, an inhibitor of the sarco/endoplasmic reticulum Ca(2+)-ATPase (SERCA)), dithiothreitol (DTT, a reducing agent) and glucose starvation activated the UPR and repressed QPRT levels in HK2 cells (**Figure 5A** to **C**), whereas other key enzymes of the NAD^+ biosynthesis and salvage pathways, including indoleamine 2,3-dioxygenase 1 (IDO1), ACMSD, nicotinic acid phosphoribosyl transferase (NAPRT) and nicotinamide phosphoribosyl transferase (NAMPT), were not affected by ER stress (**Suppl. Figure 9**). Time-course analysis of QPRT transcripts levels in HK2 cells after ER stress induction showed QPRT down regulation starting 4h after stimulation (**Figure 5D** and **E**). The transcription factor DDIT3 has a repressive activity on numerous target genes (24),(25),(26),(23), leaving the possibility that it could repress QPRT transcription. siRNA-mediated RNA interference against DDIT3 attenuated QPRT reduction upon ER stress (**Figure 5F**). The over-expression of DDIT3 in non-stressed cells had no impact on QPRT expression (**Figure 5G**), suggesting that additional factors embedded in the ER stress response are required for DDIT3 to repress QPRT. These findings were replicated in primary cultured PTCs (**Suppl. Figure 10**). Together, these results indicate that ER stress impairs QPRT expression and that DDIT3 may participate in QPRT repression.

Discussion

A better understanding of the cellular and molecular processes activated in response to kidney injury, a better characterization of the structural determinants that foster progression from AKI toward CKD, and the identification of biomarkers of ongoing tissue injury in individuals during the early stages of the disease are required to improve patient care in nephrology. Our findings link the ER stress response to fundamental changes in PTCs biology associated with AKI and AKI to CKD progression. Furthermore, this study provides a comprehensive characterization of non-invasive metabolic biomarkers of kidney disease that ultimately could be used to optimize therapies to slow disease progression.

We provide evidence for the first time that the ER stress response has a repressive role in NAD^+ biosynthesis. The relationship between ER stress and cellular energetic metabolism is

231 complex, and multiple pathways appear to be at work (27). Our results suggest a novel
232 metabolic role for the UPR in modulating NAD^+ biosynthesis, possibly mediated by DDIT3. The
233 consequences of these findings are multiple and raise several avenues for further
234 investigation. The landscape of the biological impact of de novo NAD^+ down regulation appears
235 endless given the hundreds of redox reactions involving NAD^+/NADH, and dozens of reactions
236 involving NAD^+ consumption throughout the cell (28). Considering that NAD^+ is a key
237 modulator of mitochondrial homeostasis, a prime issue to be addressed is the way the UPR
238 affects mitochondrial function and biogenesis. Indeed, the kidney is second only to the heart
239 in the abundance of mitochondria, and the elevated energetic burden may render the kidney
240 especially vulnerable to ischemia. This also implies to better understand the heterogeneity of
241 individual cellular stress responses and cell fate in face of IRI. A subset of PTCs may fail to
242 recover from acute stress and face an unresolved ER stress that may ultimately become
243 deleterious and may prompt progression toward irreversible lesions. One could envision that
244 early events that affect NAD^+ contents in a proportion of PTCs imprint a metabolic memory in
245 these cells, possibly through altered sirtuins activity and epigenetic reprogramming, and which
246 would endow them with a maladaptive phenotype, fuelling fibrogenesis, inflammation and
247 progression to CKD if a critical threshold of PTCs number is reached.

248 Our results suggest that DDIT3 could participate in the attenuation of QPRT transcription,
249 which contributes to the expanding body of data indicating that DDIT3 is not only an apoptotic
250 regulator but carries out non-apoptotic functions as well. It is clear that DDIT3 alone is not
251 sufficient to inhibit metabolic gene expression because overexpressed DDIT3 was not
252 associated with QPRT repression in the absence of ER stress. This observation suggests that
253 ER stress signals are necessary to potentiate its repressive action. Our observations are
254 reminiscent of what have been described for the suppression of genes encoding the
255 transcriptional regulators of lipid metabolism such as PPARα, or SREBF1 by DDIT3 (25),
256 raising the possibility that a regulatory program is engaged upon ER stress, and which could
257 affect metabolic genes expression in a similar manner. In the case of NAD^+ biosynthesis

impairment upon ER stress, the precise mechanisms by which DDIT3 repress QPRT upon ER stress remain to be examined in detail. This transcriptional regulation of QPRT is not exclusive, and ER stress may affect QPRT enzyme activity trough other mechanisms.

Our highlight the fact that a molecular reprogramming process occurring within a stressed cell in an injured tissue can be non-invasively detected and quantified and provide information regarding the magnitude of the damage. Implementing uQ/T as a non-invasive biomarker to improve prediction performance will provide a validated tool to increase the earliness and specificity of the diagnosis of kidney injury, which is a major prerequisite for successful intervention. It is anticipated that the earlier that therapy can be started, the greater the chances are to stop the pathological process. In agreement, the detection of increased uQ/T could lead to a better stratification of the risk of kidney disease progression. uQ/T is a new monitoring tool that could be routinely used in the follow-up of individuals with kidney disease. Individuals at high risk of disease progression will benefit from early nephroprotective strategies whose purpose is to increase intracellular NAD^+ contents, and that would slow disease progression.

In conclusion, ER stress impairs de novo NAD^+ biosynthesis and the transcription factor DDIT3 may be involved in QPRT repression. Unresolved ER stress and QPRT down regulation constitute a signature of the transition from AKI to CKD. Finally, Elevated uQ/T levels reflect the severity of tissue damage upon acute kidney allograft injury and are predictive of kidney outcomes and chronic kidney damage.

Methods

Study populations

HEGP Cardiopulmonary bypass cohort for urinary metabolome: From 17 February 2017 to 26 April 2017, 42 patients undergoing scheduled cardiac surgery with CPB were enrolled. Detailed information on the cohort is available in the Supplementary file. The exclusion criteria were: an eGFR <30 ml/min/1.73 m^2, infusion of a radio contrast agent within the 24 h before surgery, a preoperative left ventricular ejection fraction <40%, age <18 years, pregnancy, and the inability to provide consent. AKI was diagnosed according to the KDIGO Clinical Practice Guideline for AKI criteria (http://kdigo.org/) in measuring serum creatinine concentrations and urine output after the surgery. All medications acting on the renin-angiotensin system and all diuretics were stopped on the day before surgery. Lost blood was recovered using Cell Saver® Elite® (Haemonetics™, France) and re-transfused when possible. Vasotropic or inotropic agents, fluids and transfusion products were administered at the discretion of the anesthesiologist based on clinical, echocardiographic and biological findings. After surgery, all patients were transferred to the cardiovascular intensive care unit. Hemodynamic data were extracted from the Philips system using IXTREND® software version 2.1.0 FW14 (Ixellence GmbH, Germany). MAP values were recorded every 1.25 sec during the CPB procedure. Clinical data were prospectively extracted from the hospital's electronic medical records. Urine samples were collected in Corning 50-ml conical tubes and centrifuged at 2,000 *g* for 20 min within 4 h of collection. Cell pellets were conserved in 300 μL of RLT® buffer (Qiagen™, France) and stored until mRNA extraction. Supernatants and cell pellets were stored at -80°C until analysis. All clinical data and samples were de-identified. Urine samples of 41 patients were technically adequate for further analysis. These urine samples used in this study have been part of a previously published analysis (29).

Leuven Kidney transplant recipients cohort for kidney allograft RNA-seq: 41 KTR were enrolled at the University Hospitals of Leuven (12). In each case, protocol biopsy was performed at four different time points: before implantation (PRE, kidney flushed and stored in ice), after reperfusion (POST, at the end of the surgical procedure) and 3 and 12 months after transplantation. Genome-wide gene expression profiling using RNA-seq was performed in kidney allograft recipients as previously described (12). Based on RNAseq profiling of protocol biopsies, a computational model to characterize the transition from AKI to CKD has been developed, as previosuly described (12). Briefly, a pseudotime analysis including all 3-months and 12 months samples was performed to cover this transition. The pseudotime line separated into 2 branches: a branch with transcriptomes depicting the progression to fibrosis over time

(called "transition" and "progression"), and an opposite branch with transcriptomes moving toward recovery (called "recovery").

Necker kidney transplant recipients cohort for urinary metabolome: All of the consecutive patients (405) who received a kidney transplant at our center from January 2010 to June 2012 were considered for this prospective, longitudinal, single-center cohort study. The reasons for exclusion were: non-inclusion criteria (n=48), primary non-function/early graft loss (n=12), other study with urine monitoring (n=16), patients death within the first 6 months (n=7), and early loss of follow-up (n=22). Post-transplantation, urine was collected on day 10 for 237 out of 300 individuals initially included in the study. Glomerular filtration rate was measured using Iohexol clearance calculation. Urine samples were centrifuged at 1,000g for 10 min within 4 h of collection. The supernatant was collected after centrifugation and stored with protease inhibitors at -80°C. These urine samples used in this study have been part of a previously published analysis (30).

HEGP Chronic Kidney Disease cohort for urinary transcripts monitoring: Between November 2017 and February 2018, 55 consecutive individuals who were referred to the Nephrology Department at the Georges Pompidou European Hospital (Paris, France) for a kidney biopsy were evaluated for potential inclusion in the study. Indications for biopsy were estimated GFR < 60ml/min and/or proteinuria > 0.5 g/l. Kidney biopsies were only for patient care. At the time of biopsy, urine samples were collected for routine clinical chemistry analyses and stored at -80°C. Detailed information regarding the clinical, medical, demographic, biological, and histological status of the patients was collected using an information-based data warehouse.

Study approvals

HEGP Cardiopulmonary bypass cohort: this single-center, prospective, pilot study was approved by the French ethical committee on 7 February 2017 (CPP Sud Est III n° 2016-072 B) and registered under the EudraCT n° 2016-A01871-50. All patients provided written consent for study participation and for the biological analysis before inclusion.

Leuven Kidney transplant recipients cohort for kidney allograft RNA-seq: patients were enrolled at the University Hospitals of Leuven (12). Participants provided written consents, and the local ethic committee approved this consent procedure and studies of human.

Necker kidney transplant recipients cohort: This study was approved by the Ethics Committee of Ile-de-France XI (#13016), and all of the participating patients provided written informed consent.

HEGP Chronic Kidney Disease cohort. Analyses were performed anonymously. The patients were informed of the study and did not object to the use of their clinical and biological data collected within the framework of the care exclusively. Data management complies with French reference methodologies.

Animal experiments. Experiments were conducted according to French veterinary guidelines and those formulated by the European Commission for experimental animal use (L358–86/609EEC) and/or to the Guide for the Care and Use of Laboratory Animals as published by the US National Institutes of Health. Animals were fed ad libitum, had free access to water, and housed at constant ambient temperature in a 12-hour light cycle.

Urine analyses

Enzyme-linked immunosorbent assays. Urinary KIM-1 levels were quantified using the KIM-1 ELISA immunoassay (R&D Systems), NGAL using the Lipocalin-2/NGAL Quantikine® ELISA Immunoassays (R&D Systems), tissue inhibitor of metalloproteinases-2 (TIMP-2) and insulin-like growth factor-binding protein 7 (IGFBP7) using TIMP2 ELISA immunoassay (R&D Systems) and IGFBP7 ELISA immunoassay (MyBiosource) respectively, according to the manufacturer's protocol. Multiplication of the two markers ([TIMP-2]*[IGFBP7]) was performed as previously described (31). Because the distribution of the values of urinary KIM1, NGAL, RBP and TIMP2*IGFBP7 concentrations was skewed, we performed analyses using log-transformed values to obtain a Gaussian distribution, but this did not change the results of the comparative study.

Clinical chemistry analyses. The urine protein measurements were performed at the Clinical Chemistry Department of the Hôpital Européen Georges Pompidou. The urinary levels of retinol binding protein (RBP) were measured using a Siemens BN II nephelometer Analyzer II and kits from Siemens. Values considered normal were < 0.5 mg/L.

Urine mRNA processing. Urine samples from the CKD HEGP cohort were collected in Corning 50-ml conical tubes and centrifuged at 2,000 *g* for 20 mins within 4 h of collection. Cell pellets were conserved in 300 μL of RLT® buffer (Qiagen™, France) and stored until mRNA extraction. Supernatants and cell pellets were stored at -80°C until analysis. RNA was extracted from the pellets using the RNeasy mini kit® (Qiagen™) and reverse-transcribed into cDNAs using TaqMan® Reverse Transcription Reagents (Applied Biosystems™).

Targeted metabolomics

HK2 cells were washed twice with ice-cold PBS, drained, snapped-frozen in liquid nitrogen and stored at -80°C until analyses. After addition of an extraction solution made of 50%

methanol, 30% acetonitrile, and 20% water (32) (1 mL/1.10^6 cells or 500ul for 20 μl urine), the samples were vortexed for 5 min at 4°C, and then centrifuged at 16,000 g for 15 min at 4°C. The supernatants were collected and separated by liquid chromatography–mass spectrometry using SeQuant ZIC-pHilic column (Millipore). The aqueous mobile-phase solvent was 20-mM ammonium carbonate plus 0.1% ammonium hydroxide solution and the organic mobile phase was acetonitrile. The metabolites were separated over a linear gradient from 80% organic to 80% aqueous for 15 min. The column temperature was 50°C and the flow rate was 200 µl/min. The metabolites were detected across a mass range of 75-1,000 m/z using the Q-Exactive Plus mass spectrometer at a resolution of 35,000 (at 200 m/z) with electrospray ionization and polarity switching mode. Lock masses were used to insure mass accuracy below 5 ppm. The peak areas of different metabolites were determined using Thermo TraceFinder software using the exact mass of the singly charged ion and known retention time on the HPLC column. Data analysis was performed in the MetaboAnalyst 4.0 software (33).

Human kidney immunohistochemistry

Kidney biopsies were fixed in alcohol-formalin-acetic acid, dehydrated with ethanol and xylene, embedded in paraffin, and cut into 3μm sections. Samples were then deparaffinized, rehydrated and heated for 20 min at 97°C in citrate buffer. Endogenous peroxidase was inactivated by incubation for 10 min at room temperature in 0.3% H_2O_2. Sections were incubated with PBS containing 1:100 anti QPRT (orb317756, Biorbyt). Next, sections were incubated with anti-mouse antibody conjugated with peroxydase labeled polymer (Dako), then visualized with a peroxydase kit (Dako). Finally, the tissue sections were counterstained with hematoxylin.

Animal experiments

Tunicamycin injection: 12 weeks-old C57/BL6 background male mice (Charles River laboratories) were intraperitoneally injected with Tunicamycin (Sigma-Aldrich, T7765) (1 mg/kg) or vehicle (DMSO) at day 0, and mice were sacrificed 2 days post-injection (n=4-5 per condition). Total RNA was extracted form kidneys using the RNeasy Mini Kit® (Qiagen) according to the manufacturer's protocol.

Induction of Diabetes Mellitus: Twelve-week-old males of the Sv129J genetic background (Charles River laboratories) were rendered diabetic by Streptozotocin (Sigma-Aldrich, S-0130) (100 mg/kg in sodium citrate buffer pH = 4.5) intraperitoneal injection on 2 consecutive days. Control mice received citrate buffer alone. Mice with fasting glycemia above 300 mg/dL were considered diabetic. Mice were euthanized 10 weeks after the induction of diabetes. (n=3-4 per condition). Total RNA was extracted from kidneys using the RNeasy Mini Kit® (Qiagen) according to the manufacturer's protocol.

UmodC147W/+ mouse: A detailed description of the methods for the of the UmodC147W/+ mouse line of the C57BL/6J genetic background was previously reported (34). Public repositories pertaining to the transcriptome of mRNA isolated from whole-kidney tissue from mutant mice and littermate controls at multiple time points, including 12 and 24 weeks (Gene Expression Omnibus [GEO] database accession no. GSE102566) were analyzed for QPRT and DDIT3 expression.

Bilateral Ischemia reperfusion injury: this procedure has been detailed in (13). A 21-minutes warm IRI was performed, and cohorts of injured mice were examined at: 2 and 4 h; 1, and 2, and 3 days after IRI (n=3-4). Warm renal ischemia-reperfusion injury was performed on 10- to 12-week-old (25–28 g) C57BL/6CN male mice.

Bulk RNA-sequencing of kidneys after bilateral IRI.

This procedure has been detailed in (13).

Single-nucleus RNA-seq

snRNAseq data were obtained from an experimental model previously described (8). The experimental protocol is shown in **Suppl. Figure 2.** Seurat v3.2.0 in R v4 was used for analyses, including normalization, scaling, and clustering of nuclei. First, we analyzed each dataset separately and excluded nuclei with less than 150 or more than 8,000 genes detected. We also excluded nuclei with a relatively high percentage of UMIs mapped to mitochondrial genes (>1) and ribosomal genes (>1, for normal kidney sample, and > 2, all other samples). We performed curated doublet removal based on known lineage-specific markers. The samples from different datasets were integrated to avoid batch effect using Seurat standard workflow splitting by dataset. Following ScaleData, RunPCA, FindNeighbours and FindCluster at a resolution of 0.5 were performed. We focused our analysis on control and early time points post IRI (4 and 12 h) resulting in total 34,755 renal nuclei including 19,926 PTCs from 15 samples (8 controls and 7 post IRI). Cluster reassignment was performed based on manual review of lineage-specific marker expression. For data visualization we used RunUMAP, FeaturePlot, Dotplot from Seurat and dittoHeatmap from dittoSeq package.

Cells

HK2 cell line: Normal human renal epithelial cells of proximal origin (HK-2) were purchased from ATCC/LGC Standards (lot number 60352186), and cultured according to previously published method (35). HK-2 is a cell line derived from primary proximal tubule cells. HK-2 cells are cultured in Dulbecco's Modified Eagle Medium (DMEM) containing 5 μg/mL insulin, 10 μg/mL human apotransferrin, 500 ng/mL hydrocortisone, 10 ng/mL epithelial growth factor, 6.5 ng/mL triiodothyronin, 5 ng/mL sodium selenite, 1% fetal calf serum, 25 IU/mL penicillin,

25 μg/mL streptomycin and 10 mM HEPES buffer. These cells lines are Mycoplasm free (Mycoalert Mycoplasma Detection Kit, Lonza). Tunicamycin, thapsigargin, dithiotreitol, brefeldin A, and and etoposide were from Sigma Aldrich.

Primary culture: human renal epithelial cells were harvested from human nephrectomy specimens removed for renal cell carcinoma, and isolated according to previously published methods, with minor modifications (36). Fragments of non-malignant renal cortex were minced and digested with collagenase IV (250 IU/mL) for three hours at 37°C. Cells were centrifuged and the pellets washed three times with phosphate-buffered saline. Cells were then cultured in Dulbecco's Modified Eagle Medium (DMEM) containing 5 μg/mL insulin, 10 μg/mL human apotransferrin, 500 ng/mL hydrocortisone, 10 ng/mL EGF, 6.5 ng/mL triiodothyronin, 5 ng/mL sodium selenite, 1% FCS, 25 IU/mL penicillin, 25 μg/mL streptomycin and 10 mM HEPES buffer. Cells were incubated at 37°C in 5% $C0_2$ and 95% air. The characterization of our cellular model has been published previously (37), confirming the proximal descent of the vast majority of the cultured tubular epithelial cells. Experiments were not performed with cells beyond the third passage.

RNA extraction and real-time quantitative polymerase chain reaction (RT-qPCR)

Total RNA was extracted using the RNeasy Mini Kit® (Qiagen) according to the manufacturer's protocol. Transcript expression levels were quantified through SYBR green RT-qPCR using an ABI PRISM 7900 sequence detector system (Applied Biosystems). Vehicle-treated samples were used as controls, and the fold-changes for each tested gene were normalized to the Ribosomal Protein L13A (RPL13A) housekeeping gene. The relative expression levels were calculated using the $2^{(-\Delta\Delta CT)}$ method (38). By definition, the expression level of a given gene in control sample, using the $2^{-\Delta\Delta CT}$ method to calculate relative expression levels, is 1. Primers sequences are listed in the **Suppl**. **Table 1**

Protein extraction and immunoblotting

Cells were washed in PBS and incubted for 30 min at 4°C and in mPER lysis buffer (Thermo Fisher Scientific) with protease (HaltTM Protease Inhibitor Cocktail 100X, Thermo Fisher Scientific) and phosphatase inhibitors (HaltTM Phosphatase Inhibitor Cocktail 100X, Thermo Fisher Scientific). Extracts were centrifuged at 14,000 xg for 15 min. Protein concentrations in the supernatant were measured by using a Pierce BCA Protein Assay Kit (Thermo Fisher Scientific) and Tecan Safire® plate reader. Protein extracts (25 μg) were resolved by 4-12% SDS-PAGE (Invitrogen) and transferred to nitrocellulose membranes (iBlot, Invitrogen). Membranes were blocked with SEABLOCK blocking buffer (Thermo-Scientific) for 1 h at room temperature and then incubated overnight at 4°C with primary antibody diluted in blocking

buffer. Primary antibodies were anti QPRT (HPA011887, Sigma-Aldrich), anti DDIT3 (L63F7, Cell Signaling Technology), anti PARP (ref 95424, Cell Signaling Technology), anti BiP (GRP78) (sc-1050, Santa Cruz Biotechnology), anti-PERK (C33E10, Cell Signalling technology), anti eiF2α (#9722, Cell Signaling Technology), anti phospho-eiF2α (#9721, Cell Signaling Technology), anti-Tubulin (T9026, Sigma-Aldrich). After washings in PBS-Tween buffer, membranes were incubated with secondary antibody coupled to IRDye fluorophores. Infrared signal of membranes was revealed using an Odyssey detection system (Li-Cor biosciences, Lincoln, NE, USA).

siRNA transfections

The transient inactivation of DDIT3 was achieved using small interfering synthetic RNAs (siRNAs) designed and obtained from Qiagen and transfected using HiPerFect® (Qiagen) according to the manufacturer's protocol. Two different siRNA directed against the same target were transfected: Hs_DDIT3_1 FlexiTube siRNA (ref SI00059528) and Hs_DDIT3_3 FlexiTube siRNA (ref SI00059542). AllStars Negative Control siRNA (5′-AACGAUGACACGAACACACTT-3′) has no homology to any known mammalian gene, and validation has been performed using Affymetrix GeneChip arrays and a variety of cell-based assays to ensure minimal nonspecific effects on gene expression and phenotype. Cells were incubated with siRNA for 24 h before conducting the experiments.

Expression vectors

Cells were cultured at 37°C in 5% CO_2 and were studied while subconfluent. Transient transfection of the gene DDIT3_OHu16873C_pcDNA3.1(+) cloned by HindIII/BamHI in a pcDNA3.1 vector (Cat No: OHu16873C, Gene script) was performed using Lipofectamine 2000 (Invitrogen) according to manufacturer instructions. pcDNA3.1 vector was used as a control. After, 36 h of transfection, cells were harvested for mRNA and proteins preparation.

NAD measurement

The levels of NAD^+ and intracellular NADH were measured by a colorimetric enzymatic test (BioVision®, # K337-100) according to the manufacturer's protocol. The cells of a determined number of wells containing the 2.10^5 cells required for each test were washed with ice-cold PBS, lysed with 400 µL of extraction buffer by two cycles of freeze-thaw (freezing 10 min at -80°C, thaw 10 min on dry ice), harvested in tubes, vortexed for 10 s and centrifuged at 19,000 g for 5 min at 4°C. Concentrations of NAD^+ or NADH in cell lysates were measured at 450 nm against a calibration range with an Infinite 200 Plate Reader (TECAN). The levels of the dinucleotides were expressed per million cells.

PARP activity

The levels of PARP activity were measured by ELISA (PARP/Apoptosis Colorimetric Assay Kit Catalog Number: 4684-096-K, RD Systems) according to the manufacturer's protocol. 5.10^4 cells/200 µL fresh medium/well in a 96 well flat-bottom plate were incubated 24 h for ER stressors or 10 mM Etoposide. 25 µL Samples containing 200 µg proteins were evaluated in triplicate. PARP activity in samples was evaluated in semi-quantitatively detecting PAR deposited onto immobilized histone proteins in a 96-well format. An anti-PAR monoclonal antibody, goat anti-mouse IgG-HRP conjugate, and HRP substrate are used to generate a colorimetric signal (450 nm). Absorbance correlates with PARP activity.

Statistical analysis

Graphs were generated using GraphPad Prism 7 Software (GraphPad Software, Inc.). Statistical analyses were performed with JMP.10 software (SAS Institute Inc). Student's t tests were 2 tailed and one-way ANOVA was performed when indicated. A p value less than 0.05 was considered significant.

Data availability

RNA-seq data for human kidney transplant biopsies are available at GEO (GSE126805).
Transcriptomic data for human diabetic kidneys are available at GEO (GSE30122).
RNA-seq data for mouse IRI are available at GEO (GSE52004).
RNAseq data for UmodC147W/+ kidneys and UMOD-expressing epithelium are available at GEO (GSE1102566).
RNAseq and proteomic data for rat microdissected tubules are available at GEO (GSE56743 and PXD16958).
RNAseq data for renal cell lines are available at GEO (GSE135441, GSE 111837 and GSE99701).
snRNA-seq data are available at GEO (GSE151167, GSE139107, GSE163863).
Raw data of metabolomics analyses and clinical data are available from the corresponding authors upon reasonable request.

Author contributions

N.P. conceived and designed the project. N.P., Y.B., A.R. Z.N., and V.P., performed experiments. N.P. analyzed CBP datasets. I.N. performed metabolomic analyses. A.H. and P.G. validated data interpretation. O.L. provided diabetic mice kidneys. B.F and P.WR. generated the CPB database urine biocollection. A.K. generated HEGP CKD datasets. M.N. and P.E.C. provided RNA-seq data from kidney allograft recipients and P.E.C. performed analyses. D.A. generated Necker's KTR datasets and urine biocollection. P.E.C. and A.R.

conducted snRNA-seq experiments and analysis. N.P and P.E.C. wrote the manuscript. First authorship order was assigned according to the relative amount of data generated in the project in agreement with the 3 co-authors (Y.B, A.R. and Z.N.).

Acknowledgment

This work was funded by grants from the Institut National de la Santé et de la Recherche Médicale (INSERM), La Fondation du Rein (Prix Michel Olmer), and L'Agence de la Biomédecine.

References

1. Verdin E. NAD^+ in aging, metabolism, and neurodegeneration. *Science* 2015;350(6265):1208–1213.

2. Lin S-J. Requirement of NAD and SIR2 for Life-Span Extension by Calorie Restriction in Saccharomyces cerevisiae. *Science* 2000;289(5487):2126–2128.

3. Katsyuba E, et al. NAD+ homeostasis in health and disease. *Nat. Metab.* 2020;2(1):9–31.

4. Katsyuba E, et al. De novo NAD+ synthesis enhances mitochondrial function and improves health. *Nature* 2018;563(7731):354–359.

5. Ralto KM, Rhee EP, Parikh SM. NAD+ homeostasis in renal health and disease. *Nat. Rev. Nephrol.* 2020;16(2):99–111.

6. Poyan Mehr A, et al. De novo NAD+ biosynthetic impairment in acute kidney injury in humans. *Nat. Med.* 2018;24(9):1351–1359.

7. Hershberger KA, Martin AS, Hirschey MD. Role of NAD+ and mitochondrial sirtuins in cardiac and renal diseases. *Nat. Rev. Nephrol.* 2017;13(4):213–225.

8. Legouis D, et al. Altered proximal tubular cell glucose metabolism during acute kidney injury is associated with mortality. *Nat. Metab.* 2020;2(8):732–743.

9. Abedini A, et al. Urinary Single-Cell Profiling Captures the Cellular Diversity of the Kidney. *J. Am. Soc. Nephrol.* [published online ahead of print: February 2, 2021]; doi:10.1681/ASN.2020050757

10. Suthanthiran M, et al. Urinary-cell mRNA profile and acute cellular rejection in kidney allografts. *N. Engl. J. Med.* 2013;369(1):20–31.

11. Racusen LC, et al. Culture of renal tubular cells from the urine of patients with nephropathic cystinosis.. *J. Am. Soc. Nephrol.* 1991;1(8):1028–1033.

12. Cippà PE, et al. Transcriptional trajectories of human kidney injury progression. *JCI Insight* 2018;3(22). doi:10.1172/jci.insight.123151

13. Liu J, et al. Molecular characterization of the transition from acute to chronic kidney injury following ischemia/reperfusion. *JCI Insight* 2017;2(18):e94716.

14. Woroniecka KI, et al. Transcriptome Analysis of Human Diabetic Kidney Disease. *Diabetes* 2011;60(9):2354–2369.

15. Qiu L, et al. Kidney-intrinsic factors determine the severity of ischemia/reperfusion injury in a mouse model of delayed graft function. *Kidney Int.* [published online ahead of print: August 18, 2020]; doi:10.1016/j.kint.2020.07.033

16. Noh MR, et al. C/EBP homologous protein (CHOP) gene deficiency attenuates renal ischemia/reperfusion injury in mice. *Biochim. Biophys. Acta BBA - Mol. Basis Dis.* 2015;1852(9):1895–1901.

17. Fan Y, et al. Inhibition of Reticulon-1A-Mediated Endoplasmic Reticulum Stress in Early AKI Attenuates Renal Fibrosis Development. *J. Am. Soc. Nephrol. JASN* 2017;28(7):2007–2021.

18. Lee JW, Chou C-L, Knepper MA. Deep Sequencing in Microdissected Renal Tubules Identifies Nephron Segment-Specific Transcriptomes. *J. Am. Soc. Nephrol. JASN* 2015;26(11):2669–2677.

19. Limbutara K, Chou C-L, Knepper MA. Quantitative Proteomics of All 14 Renal Tubule Segments in Rat. *J. Am. Soc. Nephrol. JASN* 2020;31(6):1255–1266.

20. Harding HP, et al. An Integrated Stress Response Regulates Amino Acid Metabolism and Resistance to Oxidative Stress. *Mol. Cell* 2003;11(3):619–633.

21. Siu F, et al. ATF4 is a mediator of the nutrient-sensing response pathway that activates the human asparagine synthetase gene. *J. Biol. Chem.* 2002;277(27):24120–24127.

22. Hogan KA, Chini CCS, Chini EN. The Multi-faceted Ecto-enzyme CD38: Roles in Immunomodulation, Cancer, Aging, and Metabolic Diseases. *Front. Immunol.* 2019;10. doi:10.3389/fimmu.2019.01187

23. Oyadomari S, Mori M. Roles of CHOP/GADD153 in endoplasmic reticulum stress. *Cell Death Differ.* 2004;11(4):381–389.

24. Cao Y, et al. ER stress-induced mediator C/EBP homologous protein thwarts effector T cell activity in tumors through T-bet repression. *Nat. Commun.* 2019;10(1):1280.

25. Chikka MR, et al. C/EBP Homologous Protein (CHOP) Contributes to Suppression of Metabolic Genes during Endoplasmic Reticulum Stress in the Liver. *J. Biol. Chem.* 2013;288(6):4405–4415.

26. Ubeda M, et al. Stress-Induced Binding of the Transcription Factor CHOP to a Novel DNA Control Element. *MOL CELL BIOL* 1996;16:11.

27. Lemmer IL, et al. A guide to understanding endoplasmic reticulum stress in metabolic disorders. *Mol. Metab.* 2021;47:101169.

28. Zempleni J, et al. *Handbook of Vitamins*. CRC Press; 2013:

29. Fohlen B, et al. Real-Time and Non-invasive Monitoring of the Activation of the IRE1α-XBP1 Pathway in Individuals with Hemodynamic Impairment. *EBioMedicine* 2018;27:284–292.

30. Tavernier Q, et al. A Comparative Study of the Predictive Values of Urinary Acute Kidney Injury Markers Angiogenin and Kidney Injury Molecule 1 for the Outcomes of Kidney Allografts. *Transplant. Direct* 2017;3(9):e204.

31. Xie Y, et al. Tissue inhibitor metalloproteinase-2 (TIMP-2) • IGF-binding protein-7 (IGFBP7) levels are associated with adverse outcomes in patients in the intensive care unit with acute kidney injury. *Kidney Int.* 2019;95(6):1486–1493.

626 32. Mackay GM, et al. Analysis of Cell Metabolism Using LC-MS and Isotope Tracers.
627 *Methods Enzymol.* 2015;561:171–196.

628 33. Chong J, Wishart DS, Xia J. Using MetaboAnalyst 4.0 for Comprehensive and
629 Integrative Metabolomics Data Analysis. *Curr. Protoc. Bioinforma.* 2019;68(1):e86.

630 34. Johnson BG, et al. Uromodulin p.Cys147Trp mutation drives kidney disease by
631 activating ER stress and apoptosis. *J. Clin. Invest.* 2017;127(11):3954–3969.

632 35. Pallet N, et al. Rapamycin inhibits human renal epithelial cell proliferation: effect on
633 cyclin D3 mRNA expression and stability. *Kidney Int.* 2005;67(6):2422–2433.

634 36. Detrisac CJ, et al. Tissue culture of human kidney epithelial cells of proximal tubule
635 origin. *Kidney Int.* 1984;25(2):383–390.

636 37. Tang S, et al. Albumin stimulates interleukin-8 expression in proximal tubular epithelial
637 cells in vitro and in vivo. *J. Clin. Invest.* 2003;111(4):515–527.

638 38. Livak KJ, Schmittgen TD. Analysis of relative gene expression data using real-time
639 quantitative PCR and the 2(-Delta Delta C(T)) Method. *Methods San Diego Calif*
640 2001;25(4):402–408.

641

642

FIGURE 1

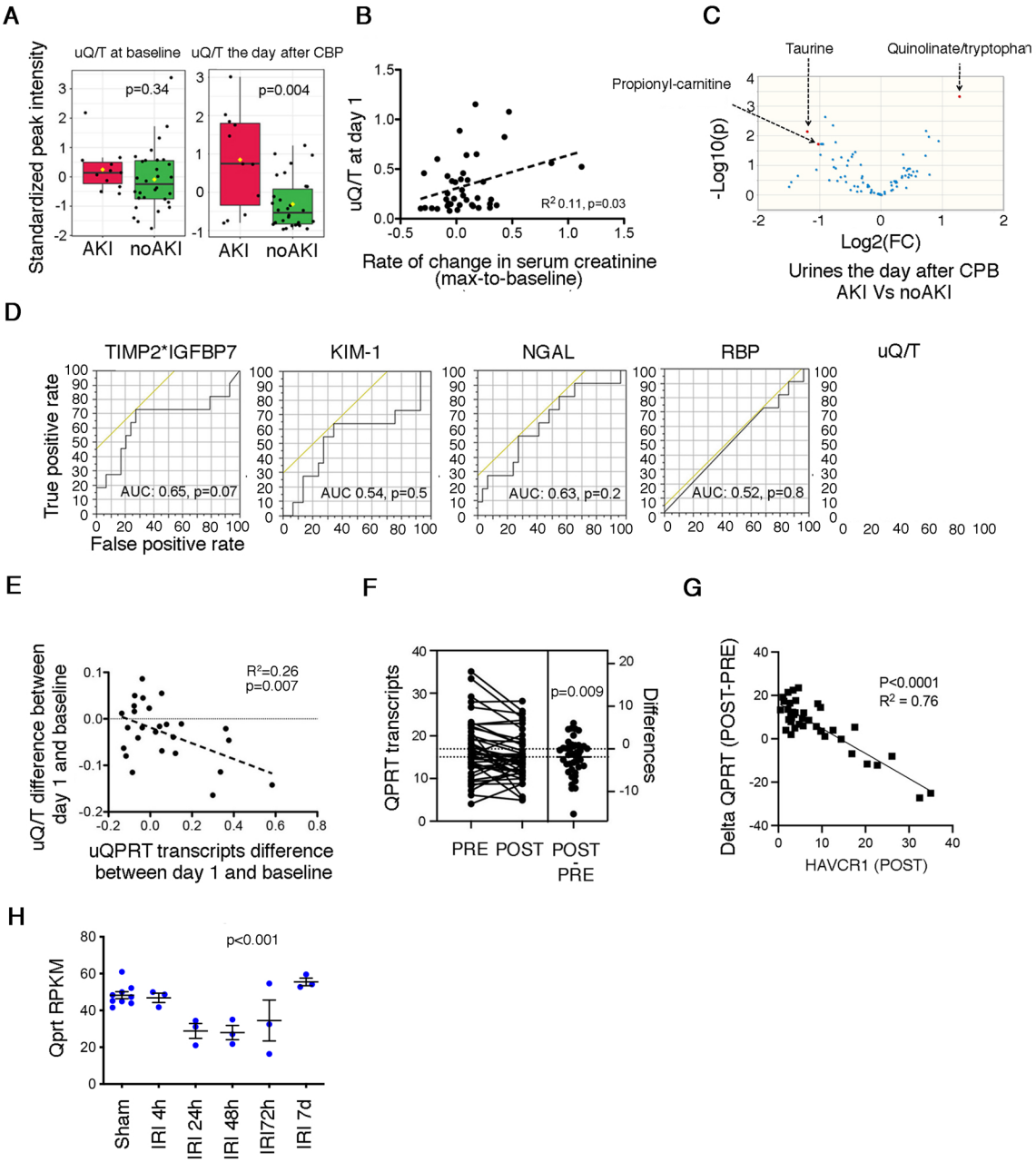
A
uQ/T at baseline
uQ/T the day after CBP
Standardized peak intensity
p=0.34
p=0.004
AKI
noAKI
AKI
noAKI
B
uQ/T at day 1
R2 0.11, p=0.03
Rate of change in serum creatinine
(max-to-baseline)
C
Taurine
Quinolinate/tryptophan
Propionyl-carnitine
-Log10(p)
Log2(FC)
Urines the day after CPB
AKI Vs noAKI
D
TIMP2*IGFBP7
KIM-1
NGAL
RBP
uQ/T
True positive rate
False positive rate
AUC: 0.65, p=0.07
AUC 0.54, p=0.5
AUC: 0.63, p=0.2
AUC: 0.52, p=0.8
E
uQ/T difference between
day 1 and baseline
R²=0.26
p=0.007
uQPRT transcripts difference
between day 1 and baseline
F
QPRT transcripts
p=0.009
Differences
PRE POST POST
PRE
G
Delta QPRT (POST-PRE)
P<0.0001
R² = 0.76
HAVCR1 (POST)
H
Qprt RPKM
p<0.001
Sham
IRI 4h
IRI 24h
IRI 48h
IRI72h
IRI 7d

Figure 1. Impaired NAD^+ biosynthesis is a very early event in AKI

A. Distribution of quinolinate/tryptophan (uQ/T) levels measured in urine at baseline, and the day after cardiopulmonary bypass (CPB), according the occurrence of AKI during the week after CPB.
B. Correlation between quinolinate/tryptophan (uQ/T) levels measured in urine the day after CPB and the rate of variation in serum creatinine between the baseline and the maximum value in the week after CPB. P value was computed with a Student's t-test.
C. Volcano plot comparing urinary metabolites of 41 patients collected 24 h after CPB and who eventually developed acute kidney injury the week after surgery.
D. Receiver operating characteristic curves for the association between the concentrations of urinary TIMP-2*IGFBP7, KIM-1, NGAL, RBP, and uQT collected the day after CPB and the occurrence of AKI the week after surgery. p values were computed with a Chi2 test, n=41.
E. Increase of uQ/T levels between the day after CPB and baseline as a function of increase of urinary QPRT transcripts levels between the day after CPB and baseline. P value was computed with a Student's t-test.
F. Expression of QPRT measured by RNA-sequencing (RNA-seq) of mRNA isolated from whole-kidney biopsies in a cohort of 42 KTR before implantation (PRE) and shortly after the restoration of the blood flow (POST). p value was computed with a Student's t-test.
G. Decrease of QPRT transcripts levels as a function of the increase in HAVCR1 transcripts levels measured by RNA-sequencing (RNA-seq) of mRNA isolated from whole-kidney biopsies in a cohort of 42 KTR shortly after the restoration of the blood flow (POST). P value was computed with a Student's t-test.
H. Expression of Qprt transcripts measured by RNA-seq of mRNA isolated from whole-mice kidneys examined at different time points following bilateral ischemia-reperfusion injury (IRI): (3 to 4 mice per condition). p value was computed with Oneway ANOVA.

FIGURE 2

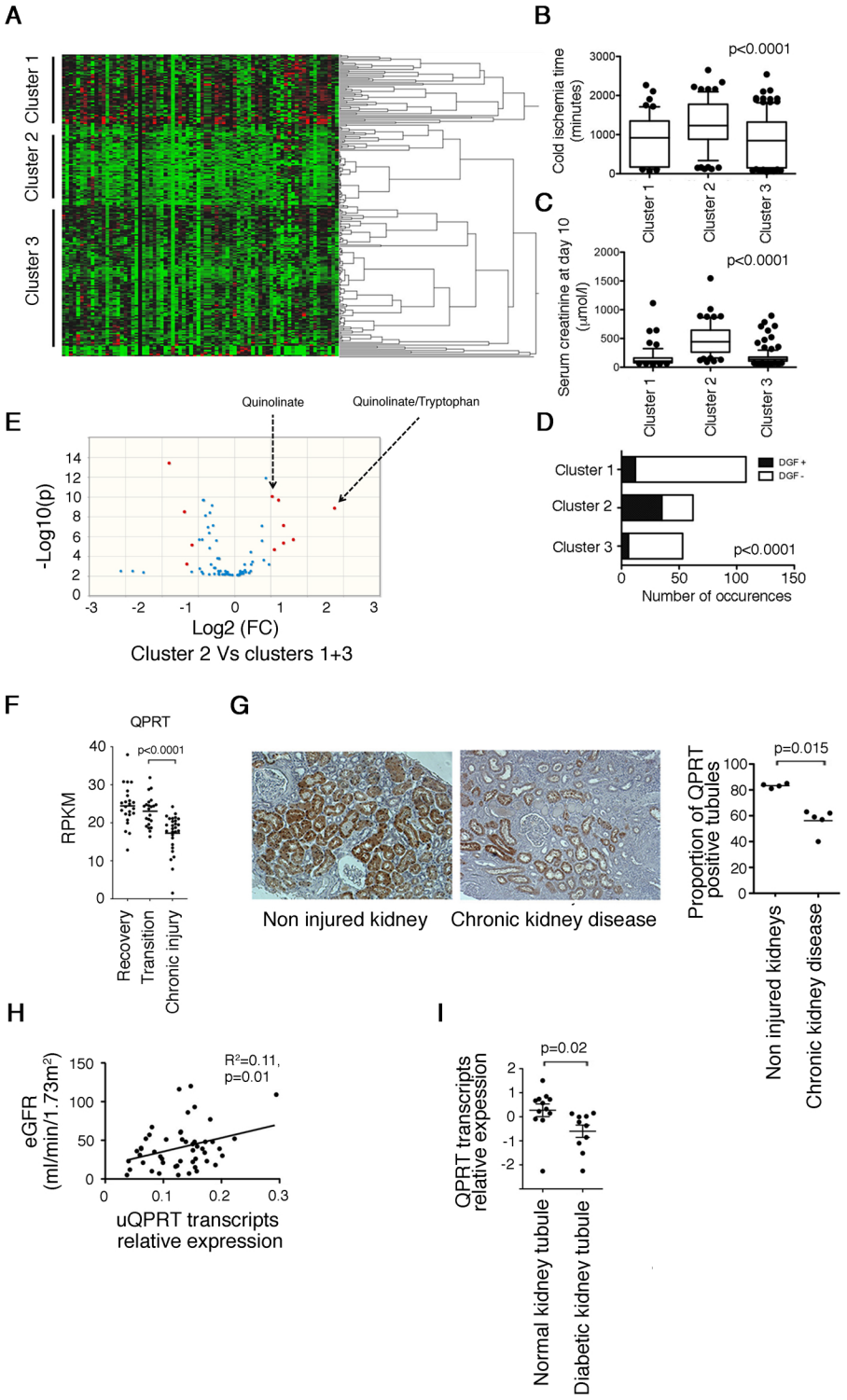
A
Cluster 1
Cluster 2
Cluster 3
B
Cold ischemia time (minutes)
p<0.0001
Cluster 1
Cluster 2
Cluster 3
C
Serum creatinine at day 10 (µmol/l)
p<0.0001
Cluster 1
Cluster 2
Cluster 3
D
Cluster 1
Cluster 2
Cluster 3
DGF +
DGF -
p<0.0001
Number of occurences
E
Quinolinate
Quinolinate/Tryptophan
-Log10(p)
Log2 (FC)
Cluster 2 Vs clusters 1+3
F
QPRT
RPKM
p<0.0001
Recovery
Transition
Chronic injury
G
Non injured kidney
Chronic kidney disease
Proportion of QPRT positive tubules
p=0.015
Non injured kidneys
Chronic kidney disease
H
eGFR (ml/min/1.73m²)
R²=0.11, p=0.01
uQPRT transcripts relative expression
I
QPRT transcripts relative expression
p=0.02
Normal kidney tubule
Diabetic kidney tubule

Figure 2. Persistent QPRT reduction is associated with progression to chronic kidney disease

A. Hierarchical clustering of 237 urine samples collected 10 days after kidney transplantation. **B.** Distribution of cold ischemia times, according to the clusters identified by hierarchical clustering in (A). p value was computed using one-way ANOVA.
C. Distribution of serum creatinine 10 days after transplantation, according to the clusters identified by hierarchical clustering in A. p value was computed using one-way ANOVA.
D. Proportion of delayed graft function (DGF, need for a dialysis session during the 7 days after transplantation) events according to the clusters identified by hierarchical clustering in A. p value was computed using one-way ANOVA.
E. Volcano plot comparing urinary metabolites of 273 patients collected 10 days after kidney transplantation in cluster 2 or clusters 1+3. Urinary quinolinate/tryptophan (uQ/T) remained significantly increased when using FDR adjusted p values.
F. Expression of QPRT measured by RNA-sequencing (RNA-seq) of mRNA isolated from whole-kidneys in the group of 42 kidney transplant recipients who recovered or progressed to fibrosis according to the computational model described in (12) which identified 2 main transcriptional trajectories leading to kidney recovery or to sustained injury with associated fibrosis and renal dysfunction. p values were computed using Student's t-test.
G. Representative photomicrograph of human QPRT expression evaluated by immunohistochemistry in kidney from an individual without chronic kidney disease (left) and advanced chronic kidney disease (right). Original magnification x40. The distributions of QPRT positive tubules sections corresponding to each condition (n=4) were compared with a Student's T test.
H. Correlation between urinary QPRT transcripts levels and eGFR in 55 patients explored for a chronic kidney disease. P value was computed with a Student's t-test.
I. Relative expression of QPRT transcripts in diabetic kidney disease tubulointerstitium samples (n=10) compared with control samples (n=12). p value was computed using Student's t-test. Data are from public repositories (NCBI accession GSE126805).

FIGURE 3

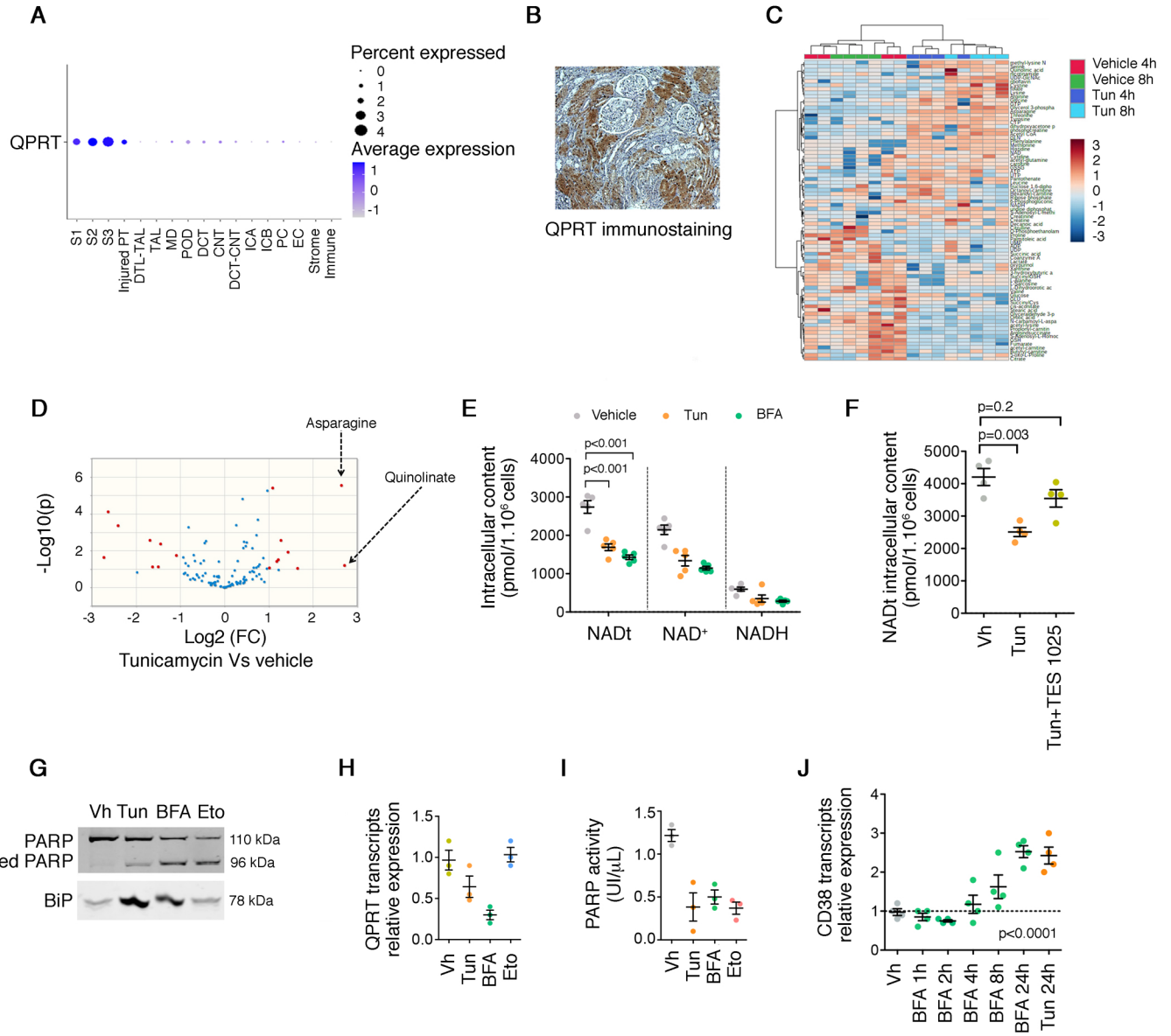
A
QPRT
Percent expressed
0
1
2
3
4
Average expression
1
0
-1
S1
S2
S3
Injured PT
DTL-TAL
TAL
MD
POD
DCT
CNT
DCT-CNT
ICA
ICB
PC
EC
Strome
Immune
B
QPRT immunostaining
C
Vehicle 4h
Vehice 8h
Tun 4h
Tun 8h
3
2
1
0
-1
-2
-3
D
Asparagine
Quinolinate
-Log10(p)
Log2 (FC)
Tunicamycin Vs vehicle
E
Vehicle
Tun
BFA
p<0.001
p<0.001
Intracellular content (pmol/1.10^6 cells)
NADt
NAD+
NADH
F
p=0.2
p=0.003
NADt intracellular content (pmol/1.10^6 cells)
Vh
Tun
Tun+TES 1025
G
Vh Tun BFA Eto
PARP
cleaved PARP
110 kDa
96 kDa
BiP
78 kDa
H
QPRT transcripts relative expression
Vh
Tun
BFA
Eto
I
PARP activity (UI/µL)
Vh
Tun
BFA
Eto
J
CD38 transcripts relative expression
p<0.0001
Vh
BFA 1h
BFA 2h
BFA 4h
BFA 8h
BFA 24h
Tun 24h

Figure 3. ER stress reduces de novo NAD^+ biosynthesis in the kidney

A. Qprt gene expression in the renal cell types identified by snRNAseq of 8 control kidney samples (25,896 cells).
B. Representative photomicrograph of human QPRT expression evaluated by immunohistochemistry in kidney. Original magnification x40.
C. Hierarchical clustering of HK2 cells incubated with 2.5 μg/mL of Tun or DMS or vehicle for 4 h and 8 h (4 replicates).
D. Volcano plot comparing urinary metabolites of HK2 cells incubated with or without 2.5 μg/mL Tun for 8 h.
E. Concentrations of total NAD concentrations, NAD^+ and NADH in HK2 cells incubated with 2.5 μg/mL Tun or 5 μg/ml BFA or DMSO for 24 h (4-5 replicates). Bars represent mean±sem. p value was computed with a Dunnett's multiple comparison test.
F. Concentrations of total NAD concentrations, NAD+ and NADH in HK2 cells incubated with 2.5 μg/mL Tun alone with or without 100 μmol/L of TES 1025 for 24 h (3-4 replicates). Bars represent mean±sem. p value was computed with a Dunnett's multiple comparison test.
G. Immunoblot representing PARP, its cleaved fragment and Bip expression in HK2 24 h after incubation with DMSO, 2.5 μg/mL Tun, 5 μg/ml BFA, or 100 μM Eto. The immunoblot shown is representative of 3 independent experiments.
H. Relative expression of QPRT measured by RT-qPCR in HK2 cells incubated with 2.5 μg/mL Tun, 5 μg/ml BFA, 100 μM Eto or DMSO for 24 h (3 replicates per condition). Bars represent mean±sem.
I. the PARylation activity of PARP in HK2 cells incubated with DMSO, 2.5 μg/mL Tun, 5 μg/ml BFA, or 100 μM Eto (3-4 replicates). Bars represent mean±sem.
J. Relative expression of CD38 measured by RT-qPCR in HK2 cells incubated with 2.5 μg/mL Tun or 5 μg/ml of BFA, or DMSO for 24 h (3-4 replicates per condition). Bars represent mean±sem. p value was computed with Oneway ANOVA.

FIGURE 4

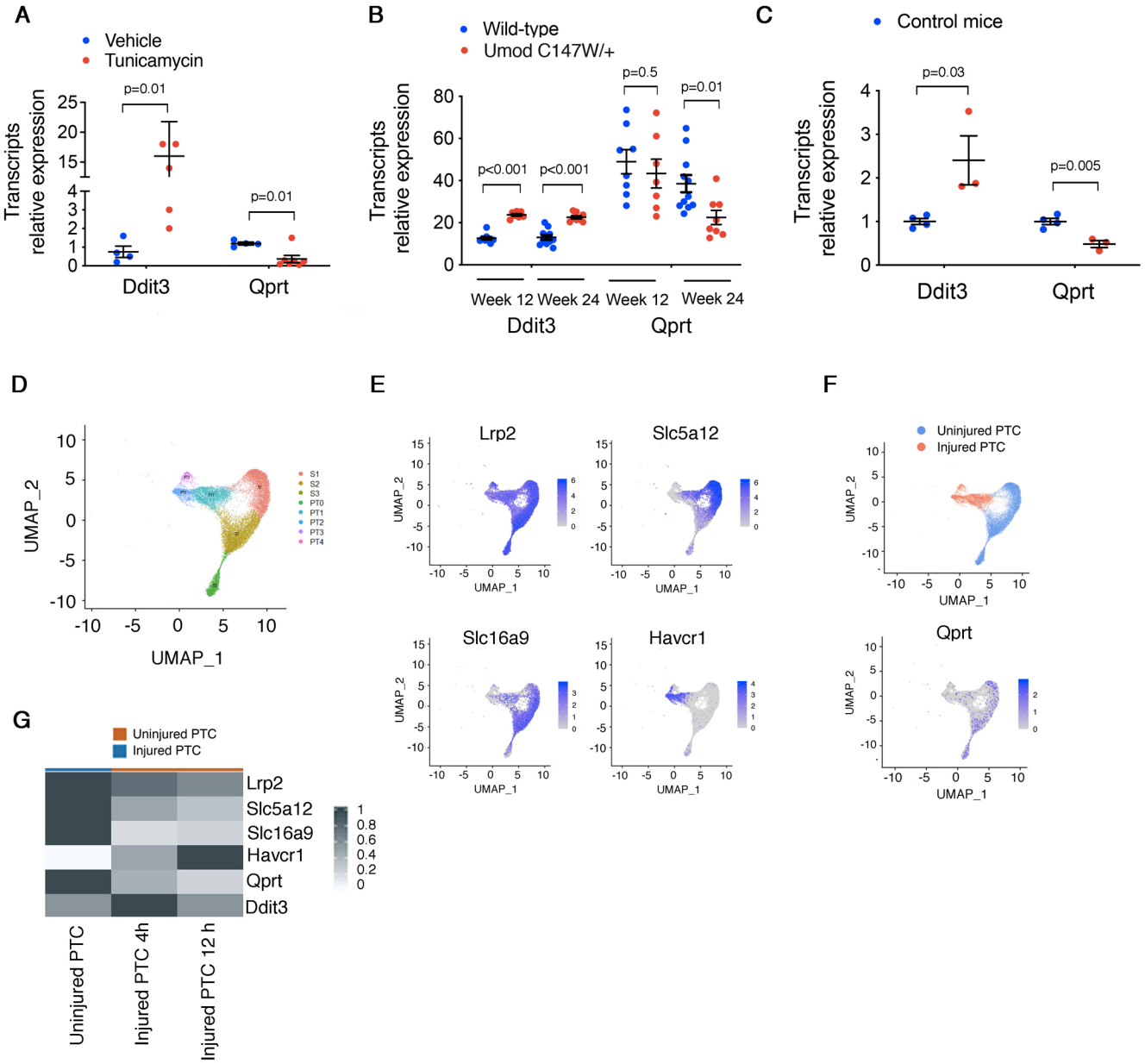
A
Vehicle
Tunicamycin
Transcripts relative expression
p=0.01
p=0.01
Ddit3
Qprt
B
Wild-type
Umod C147W/+
Transcripts relative expression
p<0.001
p<0.001
p=0.5
p=0.01
Week 12
Week 24
Week 12
Week 24
Ddit3
Qprt
C
Control mice
Transcripts relative expression
p=0.03
p=0.005
Ddit3
Qprt
D
UMAP_2
UMAP_1
S1
S2
S3
PT0
PT1
PT2
PT3
PT4
E
Lrp2
Slc5a12
Slc16a9
Havcr1
UMAP_2
UMAP_1
F
Uninjured PTC
Injured PTC
Qprt
UMAP_2
UMAP_1
G
Uninjured PTC
Injured PTC
Lrp2
Slc5a12
Slc16a9
Havcr1
Qprt
Ddit3
Uninjured PTC
Injured PTC 4h
Injured PTC 12 h

Figure 4. QPRT expression is repressed in response to kidney injuries associated with ER stress

A. Expression of Ddit3 and Qprt transcripts by q-PCR in kidneys cortex of mice 48h after intraperitoneal injection of 1 mg/kg Tun or DMSO (4 to 5 mice per condition). Bars represent mean±sem. p values were computed with a Student's t-test.
B. Expression of Ddit3 and Qprt transcripts by RNA-seq in whole-kidneys of 12 and 24 weeks old UmodC147W/+ mice and wild type mice (5 to 10 mice per condition). Data are from public repositories (NCBI accession GSE102566). Bars represent mean±sem. p values were computed with a Student's t-test.
C. Expression of Ddit3 and Qprt transcripts by q-PCR in kidneys cortex of diabetic mice. Bars represent mean±sem. p values were computed with a Student's t-test.
D. UMAPs of 7 mouse IRI and 8 control kidney samples analyzed by snRNAseq (n=19,926 cells) identify segments of the proximal tubule (S1, S2, S3) and new (injured) proximal tubule clusters (PT1, PT2, PT3).
E. UMAPs of 7 mouse IRI and 8 control kidney samples analyzed by snRNAseq (n=19,926 cells) identify the expression of differentiation markers (Lrp2, Slc5a12 and Slc16a9) and injury marker (Havcr1) in segments of the proximal tubule (S1, S2, S3) and new proximal tubule clusters (PT1, PT2, PT3)
F. (Left). UMAP of 7 mouse IRI and 8 control kidney samples analyzed by snRNAseq (n=19,926 cells) highlighting uninjured (blue) and injured proximal tubular cells (PTCs) cells (red) populations. (Right) UMAP of 7 mouse IRI and 8 control kidney samples analyzed by snRNAseq (n=19,926 cells) identify the differential expression of Qprt in injured and non-injured PTCs.
G. Expression of classical differentiation and injury markers over time after IRI in 7 mouse IRI and 8 control kidney samples analyzed by snRNAseq. Each column represents the average expression per cell state in control PTCs, injured PTCs at 4h and 12h). (n=15 samples, n=19,164 cells).

FIGURE 5

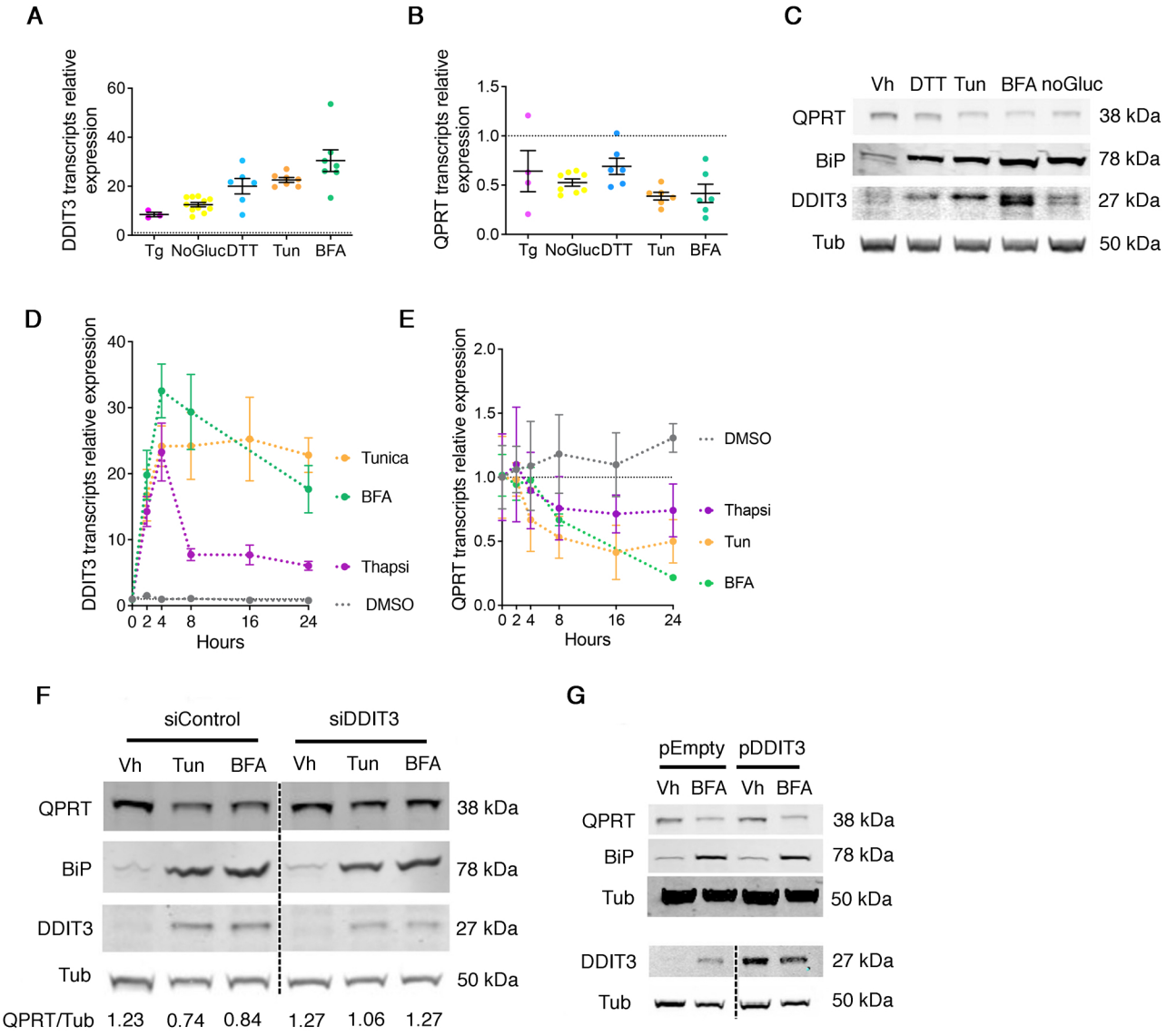
A
DDIT3 transcripts relative expression
60
40
20
0
Tg NoGlucDTT Tun BFA
B
QPRT transcripts relative expression
1.5
1.0
0.5
0.0
Tg NoGlucDTT Tun BFA
C
Vh DTT Tun BFA noGluc
QPRT
BiP
DDIT3
Tub
38 kDa
78 kDa
27 kDa
50 kDa
D
DDIT3 transcripts relative expression
40
30
20
10
0
0 2 4 8 16 24
Hours
Tunica
BFA
Thapsi
DMSO
E
QPRT transcripts relative expression
2.0
1.5
1.0
0.5
0.0
0 2 4 8 16 24
Hours
DMSO
Thapsi
Tun
BFA
F
siControl
siDDIT3
Vh Tun BFA Vh Tun BFA
QPRT
BiP
DDIT3
Tub
38 kDa
78 kDa
27 kDa
50 kDa
QPRT/Tub 1.23 0.74 0.84 1.27 1.06 1.27
G
pEmpty
pDDIT3
Vh BFA Vh BFA
QPRT
BiP
Tub
DDIT3
Tub
38 kDa
78 kDa
50 kDa
27 kDa
50 kDa

Figure 5. ER stress reduces QPRT expression in HK2 cells

A. B. Scatter dot plots representing the relative expression of DDIT3 (A) and QPRT (B) transcripts measured by RT-qPCR in HK2 cells incubated 8 h with either with 0.25 μM thaspigargin (Tg), with 1 μM dithiotreitol (DTT), with 2.5 μg/ml tunicamycin (Tun), with 5 μg/mL brefeldin A (BFA), or 48 h in a glucose-deprived culture medium (No Gluc.), and compared with vehicle (DMSO)-treated cells (6-8 replicates). The dashed line represents 1, the reference value of vehicle-treated cells. Bars represent mean±sem.

C. Immunoblot representing QPRT, BiP, DDIT3 and tubulin protein expression in HK2 24 h after incubation with DMSO (vehicle), 1 μM DTT, 2.5 μg/ml tunicamycin (Tun), with 5 μg/mL brefeldin A (BFA), or 48 h in a glucose-deprived culture medium (No Gluc.). The immunoblot shown is representative of 3 independent experiments.

D. E. Time course analysis of the relative expression of DDIT3 (D) and QPRT (E) transcripts measured by RT-qPCR in HK2 cells incubated with either with vehicle (DMSO), 0.25 μM thapsigargin (Tg), 5 μg/mL brefeldin A (BFA), or with 2.5 μg/ml tunicamycin (Tun) for up to 24 h (4 replicates). Bars represent mean±sem.

F. Immunoblot representing the expression of QPRT, BiP, DDIT3 and Tubulin proteins in HK2 cells transfected with DDIT3 siRNA (siDDIT3) or with control siRNA (siScramble) and incubated with 2.5 μg/ml tunicamycin (Tun), 5 μg/mL brefeldin A (BFA), or with DMSO (vehicle) for 24h. The immunoblot shown is representative of two independent experiments.

G. Immunoblot representing the expression of QPRT, BiP, DDIT3 and tubulin proteins in HK2 cells transfected with a pcDNA3.1 vector expressing DDIT3 or an empty vector, and incubated with 5 μg/mL brefeldin A (BFA) or with DMSO (vehicle) for 24h. The immunoblot shown is representative of two independent experiments. Bip/QPRT

Table 1. Determinants of measured glomerular filtration rate 3 months after kidney transplantation (146 KTR, living donors excluded).

Model F ratio 11.8, p<0.0001

Characteristic	Estimate	95% CI	P value
Extended criteria donor ¶ (yes)	-7.32	-10 to -4.6	<0.0001
Cold ischemia time (minutes)	-0.0001	-0.006 to 0.006	0.95
Delayed graft function ¶ ¶ (yes)	0.46	-3.3 to 4.3	0.81
Serum creatinine at day 10 (μmol/L)	-0.01	-0.03 to 0	0.048
Urinary Quinolinate-to-Tryptophan at day 10	-4.5	-8 to -1	0.01

¶ Extended criteria donors are normally aged 60 years or older, or over 50 years with at least two of the following conditions: hypertension history, serum creatinine > 133 μmol/L or cause of death from cerebrovascular accident.

¶¶ Delayed graft function (DGF) is defined as failure of the renal transplant to function immediately, with the need for dialysis in the first post-transplantation week.

Glomerular filtration rate was determined in measuring Iohexol clearance.

Table 2. Determinants of measured glomerular filtration rate 12 months after kidney transplantation (104 KTR, living donors excluded).

Characteristic	Estimate	95% CI	P value
Extended Criteria donor ¶ (yes)	-7.82	-10 to -5.2	<0.0001
Cold ischemia time (minutes)	-0.0009	-0.005 to 0.007	0.76
Delayed graft function ¶ ¶ (yes)	-1.71	-5.22 to 1.75	0.33
Serum creatinine at day 10 (μmol/L)	-0.01	-0.03 to -0.003	0.01
Urinary Quinolinate-to-tryptophan at day 10	-3.7	-6.9 to -0.61	0.02

Model F ratio 14.1, p<0.0001

¶ Extended criteria donors are normally aged 60 years or older, or over 50 years with at least two of the following conditions: hypertension history, serum creatinine > 133 μmol/L or cause of death from cerebrovascular accident.

¶¶ Delayed graft function (DGF) is defined as failure of the renal transplant to function immediately, with the need for dialysis in the first post-transplantation week.

Glomerular filtration rate was determined in measuring Iohexol clearance.